

# Quantum cascade lasers with voltage defect of less than one longitudinal optical phonon energy

Matthew D. Escarra,<sup>1,a)</sup> Anthony J. Hoffman,<sup>1</sup> Kale J. Franz,<sup>1</sup> Scott S. Howard,<sup>1,2</sup> Richard Cendejas,<sup>1</sup> Xiaojun Wang,<sup>3</sup> Jen-Yu Fan,<sup>3</sup> and Claire Gmachl<sup>1</sup>

<sup>1</sup>Department of Electrical Engineering, Princeton University, Princeton, New Jersey 08544, USA

<sup>2</sup>School of Applied and Engineering Physics, Cornell University, Ithaca, New York 14850, USA

<sup>3</sup>Adtech Optics, Inc., City of Industry, California 91748, USA

(Received 21 April 2009; accepted 27 May 2009; published online 25 June 2009)

Efficient use of applied voltage in quantum cascade (QC) lasers is a critical factor in achieving high wall-plug efficiency and low compliance voltage. We demonstrate a QC laser emitting at 4.2  $\mu\text{m}$  featuring a low voltage defect and short injector with only four quantum wells. Devices with a voltage defect of 20 meV, well below the energy of the longitudinal optical phonons, and a voltage efficiency of 91%, a record value for QC lasers, are reported for pulsed operation at 180 K. Voltage efficiencies of greater than 80% are exhibited at room temperature. Overall performance showed wall-plug efficiencies ranging from 21% at cryogenic temperatures to 5.3% at room temperature.

© 2009 American Institute of Physics. [DOI: 10.1063/1.3155429]

From environmental sensor networks to medical diagnostics and infrared countermeasures, high wall-plug efficiency (WPE) in quantum cascade (QC) lasers is essential for applications where power, temperature, weight, and space constraints exist. Furthermore, many applications favor devices with low compliance voltage for simpler and more cost-effective electronics. Recently, significant improvement has been made in the WPE of QC lasers at both cryogenic and room temperature.<sup>1–3</sup> Efforts in several areas have led to this progress, including improvement in material growth,<sup>4</sup> active core design,<sup>1,3,5,6</sup> and thermal management.<sup>1,2,6,7</sup> With regards to active core design, QC lasers provide a tremendous amount of engineering flexibility which can be exploited to optimize the desired performance characteristics. This work aims to harness this engineering flexibility to improve the WPE in QC lasers, with particular emphasis on voltage efficiency.

Voltage efficiency in a QC laser is given by

$$\eta_v = \frac{E_\gamma N_p}{N_p(E_\gamma + E_\Delta) + qV_s}, \quad (1)$$

where  $E_\gamma$  is the photon energy,  $N_p$  is the number of active/injector region periods,  $E_\Delta$  is the voltage defect per period, and  $V_s$  is the parasitic series voltage. The “voltage defect” refers to the energy drop per active/injector period that does not contribute to light generation. In choosing the voltage defect by design, one must balance two competing factors. A large voltage defect leads to excess energy drop across the structure and wasted voltage over the device. However, a small voltage defect leads to an increase in thermally activated backfilling of electrons from the injector back into the lower laser level of the preceding active region, reducing population inversion.

In this work, we maximize the voltage efficiency by reducing the voltage defect to unprecedented levels. We are able to maintain efficient lower level depopulation and avoid significant thermal backfilling through the use of lower energy states in the active regions that are even lower in energy

than the next upper laser level and hence do not contribute to the voltage defect. This allows for a voltage defect that is much smaller than the energy employed for resonant depopulation of the lower laser level. A strategy to further improve voltage efficiency involves reducing  $V_s$ , which can be done by rapid thermal annealing the metal contacts.<sup>8</sup> In contrast to previous work featuring low voltage defect QC lasers that use heterogeneous injector regions,<sup>5</sup> here we use a homogeneous design to minimize the effect of photon energy mismatch between the differing interleaved structures. We also utilize an injector region of reduced length, consisting of only four quantum wells and barriers to more rapidly move electrons through the injector into the next upper laser level. This shorter injector results in lower threshold current densities due to the increased gain of more densely packed active transitions, as well as higher maximum current and lower differential resistance due to the shorter injector transit time. Much previous work has focused on injectorless QC lasers,<sup>9</sup> including injectorless designs with a low voltage defect as low as 39 meV.<sup>10,11</sup>

A portion of this design's conduction band diagram is depicted in Fig. 1. The layer sequence of one period (in angstroms), starting from the first well in the injector, is **25/19/22/21/19/23/18/30/13/11/41/13/37/16/32/22**, where **In<sub>0.3</sub>Al<sub>0.7</sub>As** barrier layers are in bold, **In<sub>0.686</sub>Ga<sub>0.314</sub>As** well layers are plain, and the *n*-doped (Si,  $1.25 \times 10^{17} \text{ cm}^{-3}$ ) layers are underlined. The active core is designed for a photon energy of 298 meV, with a voltage defect of 36 meV at turn-on, corresponding to the resonance energy of one longitudinal optical (LO) phonon.<sup>12</sup> This defect is about half that found in conventional QC lasers at turn-on<sup>2</sup> and less than one-third of the voltage defect typically seen under normal operating conditions. Energy states below the lower laser level are spaced one and two phonon resonances lower in energy. The lowest do not contribute to the voltage defect, as there is an upward slope in the injector energy leading to the upper laser level. The injector consists of four pairs of quantum wells/barriers, compared with the seven or eight pairs used in traditional designs of similar photon energy. The total

<sup>a)</sup>Electronic mail: escarra@princeton.edu.

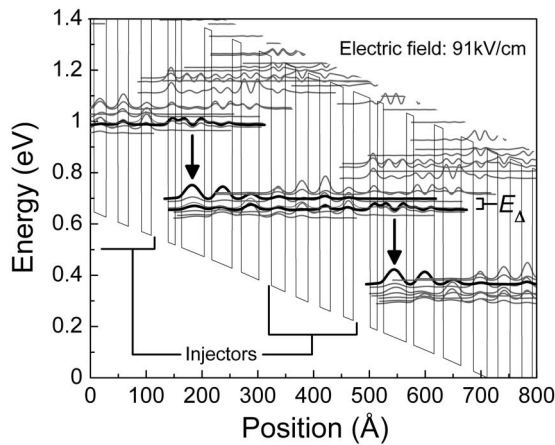


FIG. 1. A portion of the conduction band structure along with the moduli squared of the relevant wave functions. Wave functions in bold illustrate the upper and lower laser levels of each active period. The optical transition, with a design energy of 298 meV, is depicted by vertical arrows. A very low voltage defect of  $\sim 36$  meV is identified by  $E_{\Delta}$ , for an applied electric field of 91 kV/cm. One can see the shortened injector regions, consisting of four quantum wells between each set of active regions. The calculation takes the free carrier density into account through a self-consistent solution of the Schrödinger and Poisson equations.

period length is 362 Å, compared with  $\sim 500$  Å in traditional designs.<sup>6</sup>

The QC structure was grown by metal-organic chemical vapor deposition on low-doped ( $1 \times 10^{17} \text{ cm}^{-3}$ ) InP substrate using strain-balanced  $\text{In}_{0.686}\text{Ga}_{0.314}\text{As}/\text{Al}_{0.7}\text{In}_{0.3}\text{As}$ . High strain (1.1%/1.4%, respectively for InGaAs/AlInAs) was used in the well and barrier material to increase the conduction band offset and allow for high photon energy while still isolating the upper laser level from the continuum. The total structure consists of a low-loss InP waveguide (doped mostly at  $n \sim 2 \times 10^{16} \text{ cm}^{-3}$ ) surrounding 41 periods of injector/active region. Devices were fabricated as deep-etched ridge waveguide lasers of varying widths with  $\text{SiO}_2$  (3000 Å) for side-wall electrical insulation. The devices were thinned to  $\sim 200 \mu\text{m}$  and Ti/Au (200/6000 Å) top contacts and Ge/Au (200/3000 Å) bottom contacts were deposited. Ridges were cleaved to various lengths between 0.5 and 3.9 mm and mounted epitaxial side up on copper heat sinks. For continuous wave (cw) measurements, a set of devices was fabricated with electroplated gold top contacts for improved thermal conductivity. These devices were deep etched in a double-trench configuration, again using  $\text{SiO}_2$  for side-wall electrical insulation, with 8  $\mu\text{m}$  of electroplated gold on the top contact, and similar processing for the remainder of the structure.

Voltage efficiency and voltage defect are experimentally determined according to Eq. (1), where the denominator is equivalent to the total voltage drop across the structure. The photon energy was measured at various temperatures (see inset of Fig. 4). Parasitic series voltage,  $V_s$ , refers to all of the voltage drop in the structure not occurring in the active core and includes effects such as contact and wiring resistance. This parasitic voltage ranged from 0.4 V at low temperatures to 0.55 V at room temperature and was experimentally found through current-voltage measurements performed on a QC laser structure without an active core.<sup>8</sup> Pulsed light-current-voltage (LIV) measurements were performed on devices of different lengths at several heat sink temperatures. Figure 2

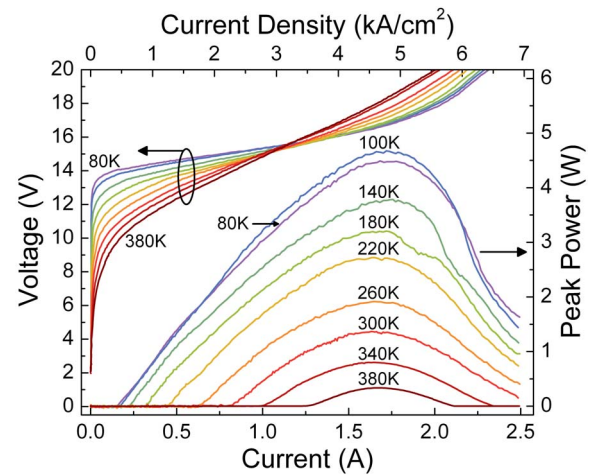


FIG. 2. (Color online) Pulsed LIV measurements for a 3 mm long and 12  $\mu\text{m}$  wide laser ridge at the indicated heat-sink temperatures. The light, showing output from both facets, is corrected for a collection efficiency of 75%.

shows results for a representative 3 mm long and 12  $\mu\text{m}$  wide ridge. This device had a low pulsed threshold current density at 80 K of 440 A/cm<sup>2</sup>, with a coincident voltage defect of only 30 meV. The voltage defect fell to less than 20 meV at 180 K. This exceptionally low value for the voltage defect is clearly below the energy of a LO phonon ( $\sim 34$  meV in this material system<sup>12</sup>), the conventional scattering mechanism for depopulation of the lower laser level in QC lasers. A voltage defect with energy corresponding to at least one LO phonon for lower laser level depopulation is generally considered essential for QC laser operation; usually two or more LO phonons are employed. Here we see that a voltage defect of much less than one LO phonon can still provide good overall laser performance.

As an indicator of performance, the WPE was measured. At 100 K, the peak WPE for a 3 mm long cavity was 21%, with a voltage defect at this peak efficiency point of 54 meV. This corresponds to values of 89% and 82% for the voltage efficiency at the threshold and peak WPE operating points, respectively. Analogous values at room temperature are 5.3% for peak WPE, 85% for voltage efficiency at threshold, and 75% for voltage efficiency at the peak WPE operating point. One can see the progression of the peak WPE, threshold voltage efficiency, and voltage efficiency at peak WPE with temperature in Fig. 3. Voltage efficiency reached as high as 91% at threshold for 180 K. The increase in voltage efficiency from low temperatures to intermediate temperatures is a result of the lowering of the voltage turn-on due to increased thermal energy of electrons moving through the structure; the subsequent drop in voltage efficiency at even higher temperatures is a consequence of exponentially rising threshold currents resulting in higher threshold voltages. To gauge cw performance, LIV measurements were performed on lasers with thick electroplated gold top contacts mounted epitaxial side up on a copper block. At 80 K, peak cw WPE was 19%, with voltage efficiency at threshold and peak efficiency of 82% and 76%, respectively. This performance is similar to that seen in pulsed operation at the same temperature.

By measuring 80 K pulsed threshold current density versus cavity length, a waveguide loss ( $\alpha_m$ ) of 1.7 cm<sup>-1</sup> was determined. Ridge widths ranging from 10 to 14  $\mu\text{m}$  were

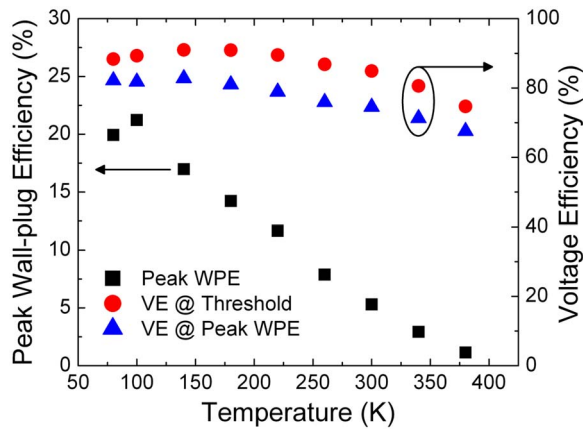


FIG. 3. (Color online) Peak WPE (squares), voltage efficiency at lasing threshold (circles), and voltage efficiency at peak WPE (triangles) vs heat-sink temperature for a 3 mm long and 12  $\mu\text{m}$  wide laser ridge under pulsed operation.

used, with no major variability in threshold current density with width. Waveguide loss was found to increase with higher temperature, as previously reported for longer wavelength QC lasers.<sup>13</sup> Considering the high voltage efficiency, low waveguide loss and low threshold currents in these devices, one would expect even higher WPE. However, the subphonon voltage defect results in relatively long injector transit times, reduced slope efficiency, and subsequently diminished WPE. The shorter length of the injector does not compensate for this effect, as other factors dominate, such as the upward slope of injector ground state energies from one active region to the next (see Fig. 1), which leads to a pooling of electrons in the lowest energy state of the active region. Another factor reducing injector transit time is the long tunneling time for the thick injection barrier.<sup>14</sup>

Figure 4 shows the temperature performance of the laser; the characteristic temperature  $T_0$  is around 118 K at lower temperatures and 174 K at higher temperatures. One would expect much lower  $T_0$  values due to considerable thermal backfilling of the lower laser level because of the low voltage defect. However, the energy levels in the active region below the lower laser level help compensate for this effect. Thus, the effective voltage defect can be as low as 20 meV while still allowing the lower laser level to depopulate through LO-phonon scattering. Still, the rise in threshold current with temperature has a distinct slowdown once the voltage defect at threshold reaches the energy of an LO phonon (see Fig. 4). This highlights the importance of a voltage defect with energy corresponding to at least one LO-phonon resonance for good high temperature performance.

In conclusion, we demonstrate a laser design approach that produces the highest reported voltage efficiency for any QC laser. This device features a short, four quantum well injector with a particularly low voltage defect (less than 20 meV), well below the energy of one LO phonon. This low voltage defect, combined with high photon energy, results in a low and room temperature voltage efficiency of 82% and 75%, respectively, at the peak WPE current. A voltage effi-

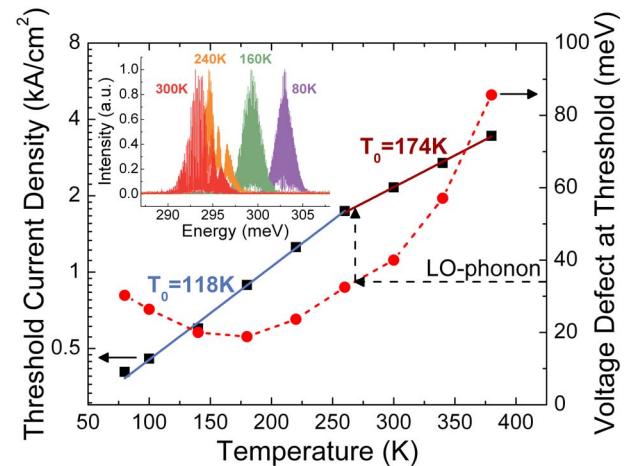


FIG. 4. (Color online) Threshold current density (black squares) and voltage defect at laser threshold (red circles) vs heat-sink temperature for a 3 mm long and 12  $\mu\text{m}$  wide laser ridge under pulsed operation. The threshold current density values are fit with exponential curves,  $J_{th} = J_0 \exp(T/T_0)$ , resulting in two regions of differing characteristic temperature  $T_0$ . A  $T_0$  of 118 K exists at lower temperatures, while a  $T_0$  of 174 K is obtained at higher temperatures. The discontinuity in the temperature performance occurs where the voltage defect at threshold corresponds to one LO phonon ( $\sim 34$  meV). The inset shows pulsed laser spectra for the device at 1.1 times threshold current for various heat-sink temperatures.

ciency as high as 91% is exhibited near threshold for intermediate temperatures. Furthermore, low threshold current densities and low waveguide loss show promise for improved overall performance.

This work is supported in part by DARPA-EMIL and MIRTHE (NSF-ERC Grant No. EEC-0540832).

<sup>1</sup>A. Lyakh, C. Pflügl, L. Diehl, Q. J. Wang, F. Capasso, X. J. Wang, J. Y. Fan, T. Tanbun-Ek, R. Maulini, A. Tsekoun, R. Go, and C. K. N. Patel, *Appl. Phys. Lett.* **92**, 111110 (2008).

<sup>2</sup>Y. Bai, S. Slivken, S. R. Darvish, and M. Razeghi, *Appl. Phys. Lett.* **93**, 021103 (2008).

<sup>3</sup>P. Q. Liu, A. J. Hoffman, M. D. Escarra, K. J. Franz, J. B. Khurgin, Y. Dikmelik, X. Wang, J. Y. Fan, and C. F. Gmachl (unpublished).

<sup>4</sup>X. Wang, J. Fan, T. Tanbun-Ek, and F.-S. Choa, *Appl. Phys. Lett.* **90**, 211103 (2007).

<sup>5</sup>A. J. Hoffman, S. S. Howard, K. J. Franz, F. Towner, and C. Gmachl, *Opt. Express* **15**, 15818 (2007).

<sup>6</sup>A. Evans, S. R. Darvish, S. Slivken, J. Nguyen, Y. Bai, and M. Razeghi, *Appl. Phys. Lett.* **91**, 071101 (2007).

<sup>7</sup>M. Beck, D. Hofstetter, T. Aellen, J. Faist, U. Oesterle, M. Illegems, E. Gini, and H. Melchior, *Science* **295**, 301 (2002).

<sup>8</sup>M. D. Escarra, S. S. Howard, A. J. Hoffman, X. Wang, and C. Gmachl (unpublished).

<sup>9</sup>M. C. Wanke, F. Capasso, C. Gmachl, A. Tredicucci, D. L. Sivco, A. L. Hutchinson, S. N. G. Chu, and A. Y. Cho, *Appl. Phys. Lett.* **78**, 3950 (2001).

<sup>10</sup>S. Katz, A. Vizbaras, G. Boehm, and M.-C. Amann, *Appl. Phys. Lett.* **94**, 151106 (2009).

<sup>11</sup>D. Dey, W. Wu, O. G. Memis, and H. Mohseni, *Appl. Phys. Lett.* **94**, 081109 (2009).

<sup>12</sup>K. J. Nash, M. S. Skolnick, and S. J. Bass, *Semicond. Sci. Technol.* **2**, 329 (1987).

<sup>13</sup>Z. Liu, C. F. Gmachl, L. Cheng, F. S. Choa, F. J. Towner, X. Wang, and J. Fan, *IEEE J. Quantum Electron.* **44**, 485 (2008).

<sup>14</sup>J. B. Khurgin, Y. Dikmelik, P. Q. Liu, A. J. Hoffman, M. D. Escarra, K. J. Franz, and C. F. Gmachl, *Appl. Phys. Lett.* **94**, 091101 (2009).